EXTENDED PDF FORMAT
SPONSORED BY
Travel Grants to the 15th International Congress of Immunology Apply Now!
www.rndsystems.com

53BP1 Regulates DSB Repair Using Rif1 to Control 5′ End Resection

Michal Zimmermann *et al.*

Science **339**, 700 (2013);
DOI: 10.1126/science.1231573

This copy is for your personal, non-commercial use only.

If you wish to distribute this article to others, you can order high-quality copies for your colleagues, clients, or customers by clicking here.

Permission to republish or repurpose articles or portions of articles can be obtained by following the guidelines here.

The following resources related to this article are available online at www.sciencemag.org (this information is current as of April 12, 2013):

Updated information and services, including high-resolution figures, can be found in the online version of this article at:
http://www.sciencemag.org/content/339/6120/700.full.html

Supporting Online Material can be found at:
http://www.sciencemag.org/content/suppl/2013/01/10/science.1231573.DC1.html

A list of selected additional articles on the Science Web sites **related to this article** can be found at:
http://www.sciencemag.org/content/339/6120/700.full.html#related

This article **cites 28 articles**, 9 of which can be accessed free:
http://www.sciencemag.org/content/339/6120/700.full.html#ref-list-1

This article has been **cited by** 2 articles hosted by HighWire Press; see:
http://www.sciencemag.org/content/339/6120/700.full.html#related-urls

This article appears in the following **subject collections:**
Molecular Biology
http://www.sciencemag.org/cgi/collection/molec_biol

Downloaded from www.sciencemag.org on April 12, 2013

Science (print ISSN 0036-8075; online ISSN 1095-9203) is published weekly, except the last week in December, by the American Association for the Advancement of Science, 1200 New York Avenue NW, Washington, DC 20005. Copyright 2013 by the American Association for the Advancement of Science; all rights reserved. The title *Science* is a registered trademark of AAAS.

53BP1 Regulates DSB Repair Using Rif1 to Control 5′ End Resection

Michal Zimmermann,[1,2] Francisca Lottersberger,[1] Sara B. Buonomo,[3] Agnel Sfeir,[1]* Titia de Lange[1]†

The choice between double-strand break (DSB) repair by either homology-directed repair (HDR) or nonhomologous end joining (NHEJ) is tightly regulated. Defects in this regulation can induce genome instability and cancer. 53BP1 is critical for the control of DSB repair, promoting NHEJ, and inhibiting the 5′ end resection needed for HDR. Using dysfunctional telomeres and genome-wide DSBs, we identify Rif1 as the main factor used by 53BP1 to impair 5′ end resection. Rif1 inhibits resection involving CtIP, BLM, and Exo1; limits accumulation of BRCA1/BARD1 complexes at sites of DNA damage; and defines one of the mechanisms by which 53BP1 causes chromosomal abnormalities in Brca1-deficient cells. These data establish Rif1 as an important contributor to the control of DSB repair by 53BP1.

The DNA damage response protein 53BP1 can influence the type of DNA repair at double-strand breaks (DSBs) (*1*) as seen in immunoglobulin gene rearrangements (*2*–*4*) and in the fusion of telomeres rendered dysfunctional through the removal of the shelterin protein TRF2 (*5*), where 53BP1 enhances the mobility of damaged telomeres, thus potentially promoting the chance of telomere-telomere encounters. In Brca1-deficient cells, 53BP1 enhances aberrant nonhomologous end joining (NHEJ) events that create lethal radial chromosomes in response to poly(ADP-ribose) polymerase PARP1 inhibitors (PARPi) (*6*). In this setting, 53BP1 may favor NHEJ-mediated misrejoining by blocking the DSB resection needed for homology-directed repair (HDR) (*6*, *7*). 53BP1 was shown to impede 5′ end resection at dysfunctional telomeres lacking all shelterin proteins and, similarly, telomeres lacking only TRF2 show evidence of 53BP1-dependent protection from resection (*5*, *8*). Based on the finding that an allele of 53BP1 (53BP1^{28A}) lacking all potential ataxia telangiectasia mutated (ATM)/ATM and Rad3-related (ATR) kinase S/TQ target sites did not support immunoglobulin class switch recombination (CSR) and failed to generate radial chromosomes in Brca1-deficient cells (*7*), it appears that these functions of 53BP1 involve interacting partner(s) modulated by the S/TQ sites. One candidate 53BP1-interacting factor is Rif1, which localizes to DSBs and dysfunctional telomeres, in a manner that is dependent on ATM signaling (*9*–*11*). Rif1 was originally identified as part of the telomeric complex in budding yeast (*12*) and was recently shown to inhibit resection at yeast telomeres (*13*, *14*). In contrast, mammalian Rif1 has no known function at functional telomeres but contributes to the intra–S phase checkpoint, facilitates recovery from replication stress, and affects replication timing (*10*, *15*–*17*).

We introduced 53BP1^{28A} and other 53BP1 mutant alleles (*7*) into immortalized TRF2$^{F/-}$53BP1$^{-/-}$ mouse embryo fibroblasts (MEFs) and induced telomere dysfunction by deletion of TRF2 (Fig. 1, A and B). The results showed that the S/TQ sites were required for the accumulation of Rif1 at deprotected telomeres, whereas the GAR, BRCT, and oligomerization domains of 53BP1 were not

[1]Laboratory for Cell Biology and Genetics, Rockefeller University, New York, NY 10065, USA. [2]Central European Institute of Technology and Faculty of Science, Masaryk University, Brno, Czech Republic. [3]European Molecular Biology Laboratory, Mouse Biology Unit, Monterotondo, Italy.

*Present address: Developmental Genetics Program and Department of Cell Biology, Skirball Institute, New York University School of Medicine, New York, NY 10016, USA.
†To whom correspondence should be addressed. E-mail: delange@mail.rockefeller.edu

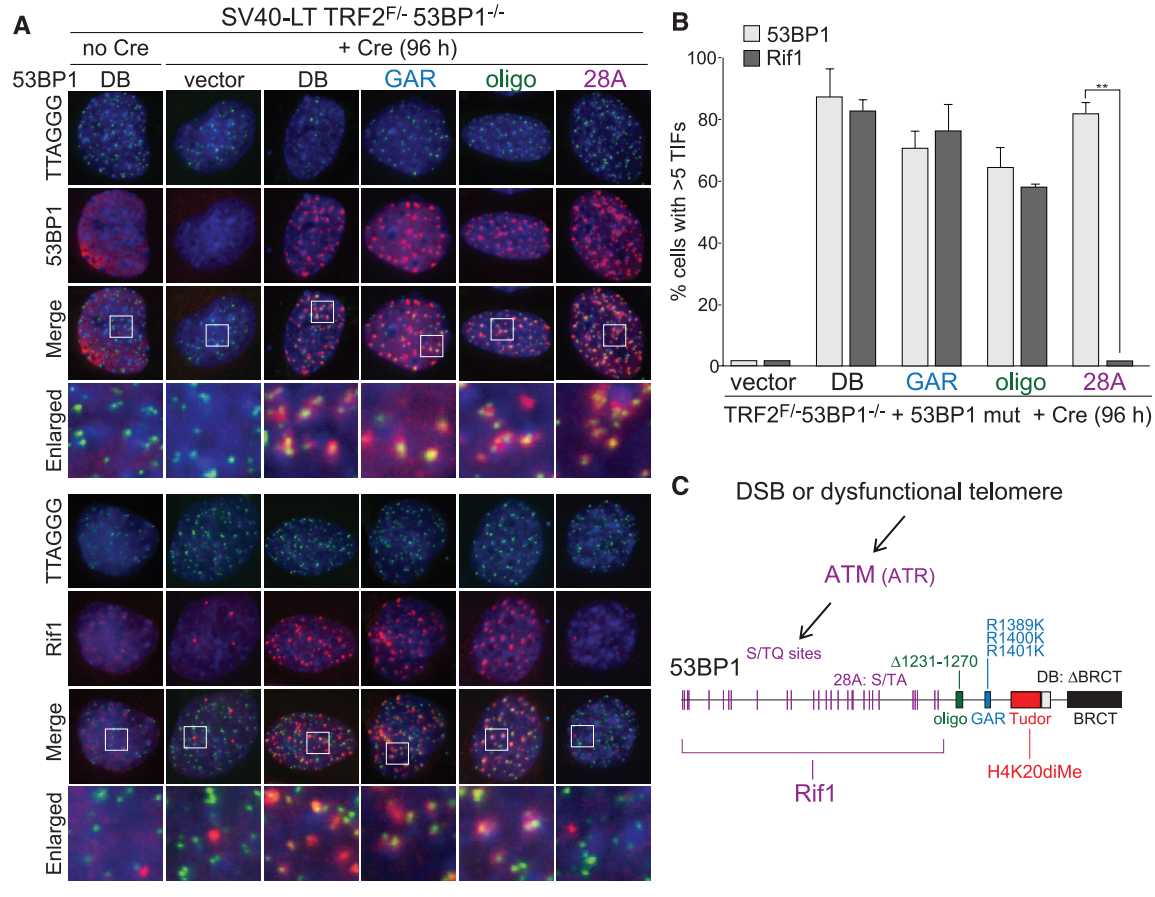

Fig. 1. Rif1 recruitment requires the S/TQ ATM/ATR target sites of 53BP1. (**A**) Detection of 53BP1 and Rif1 at dysfunctional telomeres in Cre-treated SV40 large T antigen (SV40-LT) immortalized TRF2$^{F/-}$53BP1$^{-/-}$ MEFs expressing 53BP1 mutant alleles [shown in (C)]. Indirect immunofluorescence (IF) for 53BP1 and Rif1 (red) was combined with telomeric TTAGGG fluorescence in situ hybridization (FISH) (green). Blue: 4′,6-diamidino-2-phenylindole DNA stain. (**B**) Quantification of 53BP1 and Rif1 telomere dysfunction–induced foci (TIFs) (*21*) detected as in (A). Data represent means of three experiments ±SDs (≥70 cells per experiment). **, $P < 0.05$ (two-tailed paired Student's *t* test). (**C**) Schematic of the 53BP1 mutant alleles and the role of the N-terminal S/TQ sites in the recruitment of Rif1.

Downloaded from www.sciencemag.org on April 12, 2013

(Fig. 1, A to C, and fig. S1). The functional importance of the Rif1-53BP1 interaction was addressed using a telomere-based assay system that previously uncovered the role of 53BP1 in stimulating telomeric NHEJ and protecting telomere ends from 5′ resection (*5*, *8*). Using TRF2/Rif1 conditional double-knockout MEFs, we documented a significant reduction in the incidence and rate of telomere fusions in cells lacking Rif1 (Fig. 2, A to C, and fig. S2A). This reduced NHEJ rate was not due to changes in cell cycle progression or diminished activation of the ATM kinase pathway by the deprotected telomeres (fig. S2, B to G).

As 53BP1 increases the mobility of dysfunctional telomeres, we determined whether Rif1 contributes to this aspect of 53BP1 by live-cell imaging of mCherry fused to the 53BP1 Tudor domain, which targets this marker to dysfunctional telomeres (fig. S2H). As expected, traces of the mCherry marker demonstrated that 53BP1 deficiency reduced the mobility of dysfunctional telomeres (Fig. 2D). In contrast, absence of Rif1 did not affect the mobility of the deprotected telomeres. Thus, Rif1 is not required for the 53BP1-dependent increase in the mobility of dysfunctional telomeres.

We next determined whether Rif1 contributes to the inhibition of 5′ end resection by 53BP1. When TRF2 is deleted from cells lacking 53BP1, there is a 2- to 3-fold increase in the telomeric 3′ overhang signal (*5*) which can be detected based on annealing a telomeric oligonucleotide to native telomeric DNA (Fig. 3). As expected, deletion of TRF2 resulted in the removal of the overhangs concomitant telomere fusion, whereas the overhang signal increased 3-fold when TRF2 was deleted from 53BP1-deficient cells in which telomeric NHEJ is rare and 5′ end resection is uninhibited (Fig. 3, A and B). Deletion of TRF2 from Rif1-deficient cells also resulted in an increase in the overhang signal (Fig. 3B). However, the increase was less compared to that observed in the 53BP1-deficient cells. Because the difference might be due to the lower rate of telomere fusions in the 53BP1-deficient setting, we generated immortalized $TRF2^{F/F}Lig4^{-/-}Rif1^{F/F}$ cells, which, owing to the absence of DNA ligase IV, have the same low telomere fusions rates as $TRF2^{F/-}53BP1^{-/-}$ cells (*5*). When NHEJ was blocked, the telomeric overhang increase in the Rif1-deficient cells was the same as that which occurred in the 53BP1-deficient cells (Fig. 3, C and D). The increase in overhang signal was demonstrably due to 3′ terminal sequences because the signal was removed by digestion with the *Escherichia coli* 3′ exonuclease ExoI (fig. S3A). These data suggest that Rif1 is the main factor acting downstream of 53BP1 to inhibit the resection at telomeres that lack TRF2 protection.

At telomeres that are deprived of both TRF1 and TRF2 and therefore lack all shelterin proteins, 53BP1 blocks extensive 5′ end resection that involves CtIP, BLM, and Exo1 (*8*). To test the ability of Rif1 to inhibit resection at such shelterin-free telomeres, we generated immortalized $TRF1^{F/F}TRF2^{F/F}Rif1^{F/F}$ MEFs. As expected, deletion of TRF1 and TRF2 resulted in frequent telomere fusions and nearly complete loss of the telomeric overhang signal when Rif1 was present (Fig. 3, E and F). When Rif1 was codeleted with TRF1 and TRF2, telomere fusions were also frequent, resulting in most telomeric restriction fragments shifting to a higher molecular weight (Fig. 3E). However, the telomeres that had not fused at the time point analyzed showed a notable increase in overhang signal (Fig. 3, E and F). This increase in the signal was diminished when cells were treated with short hairpin RNAs (shRNAs) against CtIP, BLM, or Exo1 (Fig. 3, G and H, and fig. S3, B and C). Thus, like 53BP1, Rif1 inhibits 5′ end resection that involves CtIP, BLM, and Exo1.

We next asked whether Rif1 affects resection at zeocin-induced DSBs by monitoring the formation of replication protein A (RPA) foci (Fig. 4A and fig. S4A). The absence of either Rif1, 53BP1, or both did not affect zeocin-induced γ-H2AX foci or the basal level of cells containing γ-H2AX foci, which likely represent replicating cells (Fig. 4, A and B). However, in zeocin-treated cells, the absence of either Rif1 or 53BP1 resulted in a significant increase in γ-H2AX foci that colocalized with RPA (Fig. 4, A and C). When either 53BP1 or Rif1 were absent, there also was a significant increase in γ-H2AX foci containing RPA in cells not treated with zeocin, presumably reflecting a higher level of resection at stalled replication forks (Fig. 4, A and C). Examination of the RPA/γ-H2AX foci in zeocin-treated

Downloaded from www.sciencemag.org on April 12, 2013

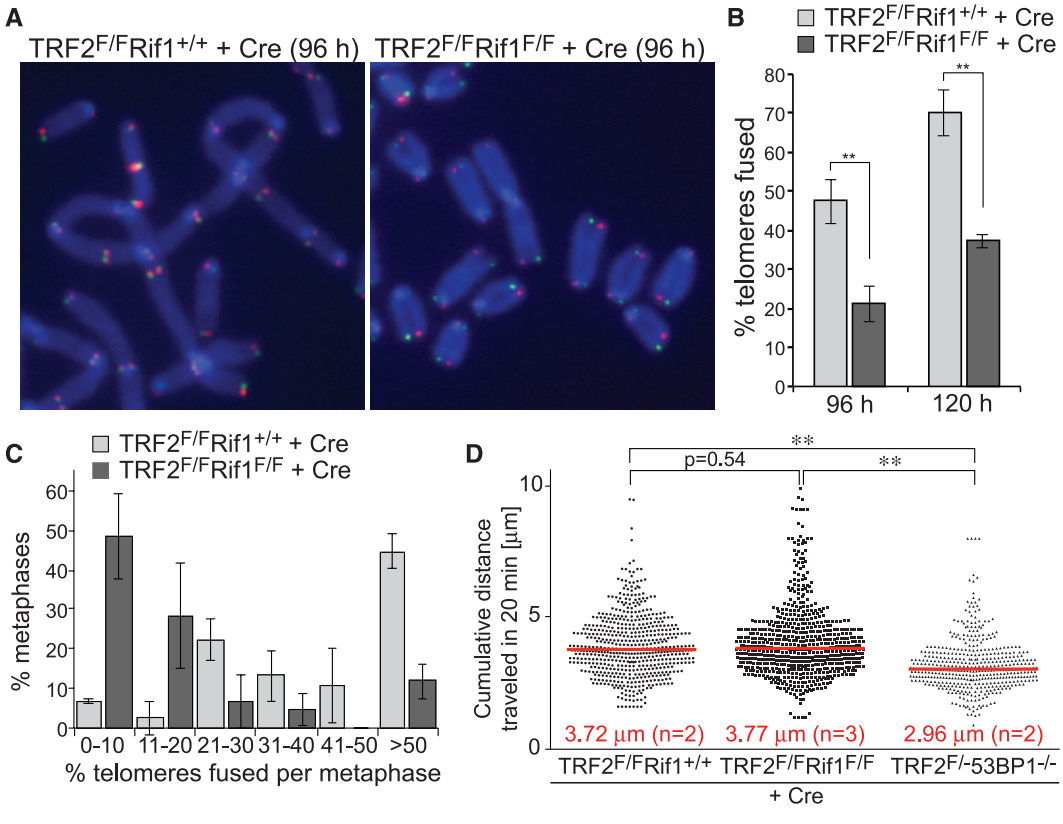

Fig. 2. Rif1 promotes telomeric NHEJ without affecting telomere mobility. (**A**) Metaphase chromosomes of Cre-treated SV40-LT immortalized $TRF2^{F/F}Rif1^{+/+}$ and $TRF2^{F/F}Rif1^{F/F}$ MEFs showing NHEJ-mediated telomere fusions detected by *chromosome orientation* FISH. Telomeres synthesized by leading-end DNA synthesis are in red; lagging-end telomeres are in green. (**B**) Quantification of telomere fusions as determined in (A) at 96 and 120 hours after Cre. Data represent means of three independent experiments ±SDs (>3000 telomeres per experiment). **, $P < 0.01$ based on two-tailed paired Student's *t* test. (**C**) Distributions of telomere fusions per metaphase at 96 hours after Cre for experiments shown in (B). (**D**) Distribution of cumulative distances traveled by mCherry-$53BP1^{1220\text{-}1711}$ foci in the indicated cell lines. Red lines represent medians. **, $P < 0.0001$ (two-tailed Mann-Whitney test).

Rif1/53BP1 double-knockout cells indicated that Rif1 and 53BP1 are epistatic in this regard because the induction of RPA/γ-H2AX foci in absence of 53BP1 was the same as in Rif1-deficient cells and the absence of both Rif1 and 53BP1 did not further increase the response (Fig. 4C). The simplest interpretation of these data is that Rif1 is the main factor acting downstream of 53BP1 to block 5′ end resection at the zeocin-induced DSBs.

Because the 53BP1/Rif1 control affects CtIP, which is thought to be delivered by a complex containing BRCA1 (*18*–*20*), we also determined whether 53BP1 and Rif1 had an effect on the presence of the BRCA1 at zeocin-induced DSBs. Using an antibody to the constitutive BRCA1 partner BARD1, we found that absence of Rif1 or 53BP1 resulted in a significant increase in the accumulation of BRCA1 complexes at zeocin-induced DSBs (Fig. 4, E and F). Consistent with the data above, Rif1 and 53BP1 were again epistatic in this regard. The absence of 53BP1 resulted in the same phenotype as absence of Rif1, and the double knockout did not show an additional increase in the incidence of BARD1 foci (Fig. 4, E and F). The absence of Rif1 also resulted in an increase in the presence of BARD1 at dysfunctional telomeres (fig. S4, B to D).

Because 53BP1 mediates the formation of misrejoined and radial chromosomes in PARPi-treated Brca1-deficient cells, we asked to what extent Rif1 is responsible for this effect. Cells lacking Rif1, 53BP1, or both were treated with a BRCA1 shRNA and the PARP inhibitor, and misrejoined chromosomes were quantified (Fig. 4, G and H). The data show the previously documented decrease in the frequency of chromosome misrejoining when 53BP1 is absent. Interestingly, absence of Rif1 also lowers the frequency of chromosome misrejoining, but the effect is significantly less than for 53BP1. Thus, the formation of misrejoined chromosomes in PARPi-treated Brca1-deficient cells is due to two distinct attributes of 53BP1, one of which requires Rif1 function.

These data identify Rif1 as the major factor acting downstream of 53BP1 in the control of 5′

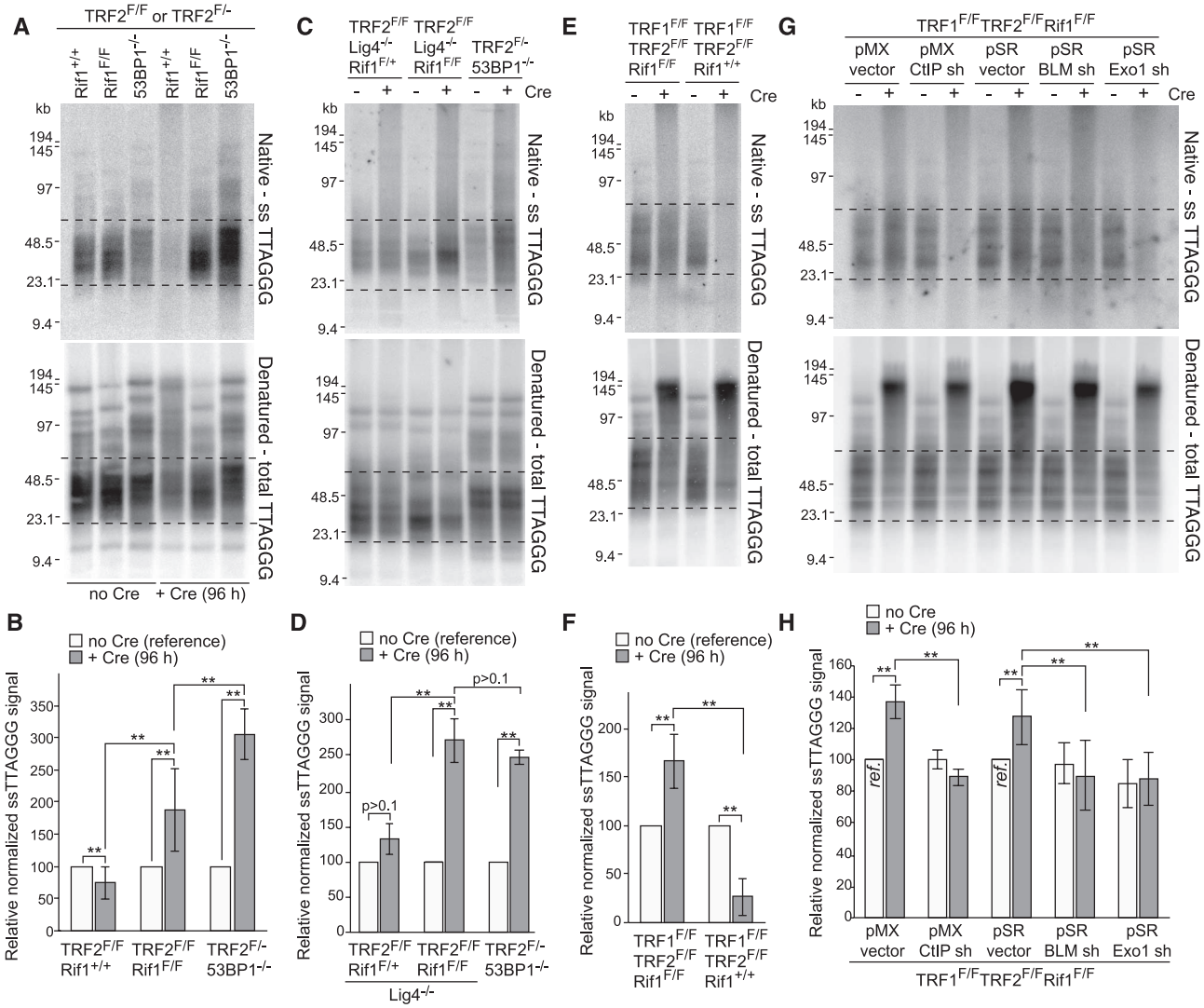

Fig. 3. Rif1 blocks 5′ end resection at dysfunctional telomeres. (**A**) Telomeric overhang assays on TRF2$^{F/F}$Rif1$^{+/+}$, TRF2$^{F/F}$Rif1$^{F/F}$ and TRF2$^{F/-}$53BP1$^{-/-}$ MEFs. Native in-gel hybridization of MboI/AluI digested DNA with end-labeled $[AACCCT]_4$ (top) and re-hybridization with the same probe after denaturation in situ (bottom). Dashed lines represent the bulk of free (unfused) telomeres used for quantification. (**B**) Quantification of overhang assays as in (A). Overhang signals in no Cre samples was set at 100%. (**C** and **D**) Overhang assays on TRF2$^{F/F}$Rif1$^{F/+}$Lig4$^{-/-}$, TRF2$^{F/F}$Rif1$^{F/F}$Lig4$^{-/-}$, and TRF2$^{F/-}$53BP1$^{-/-}$ MEFs and quantification as in (B). (**E** and **F**) Overhang assays on TRF1$^{F/F}$TRF2$^{F/F}$Rif1$^{+/+}$ and TRF1$^{F/F}$TRF2$^{F/F}$Rif1$^{F/F}$ MEFs and quantification. (**G** and **H**) Overhang assays to measure dependency on CtIP, BLM, and Exo1 and quantification. Cells infected with either pMX or pSR with or without the indicated shRNAs and treated with Cre for 96 hours. Samples with empty vectors and no Cre (*ref.*) were used as references. Data in [(B), (D), (F), and (H)] represent means of ≥3 experiments ±SDs. **, $P < 0.05$ (two-tailed paired Student's *t* test). MEFs are SV40-LT immortalized.

Downloaded from www.sciencemag.org on April 12, 2013

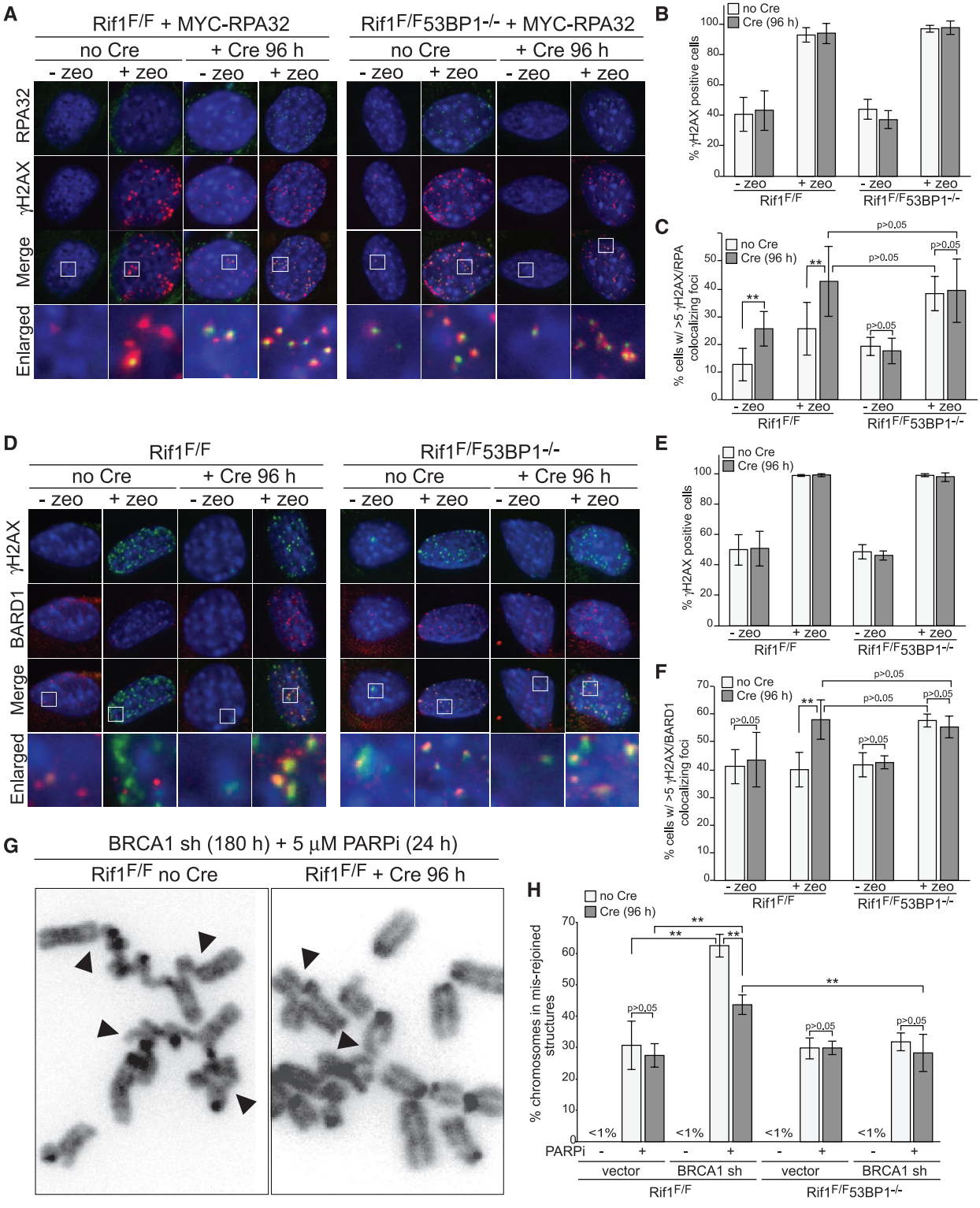

Fig. 4. Rif1 inhibits resection at DSBs and promotes radial formation. (**A**) IF for γ-H2AX (red) and MYC-RPA32 (green) in Cre-treated SV40-LT immortalized Rif1$^{F/F}$ and Rif1$^{F/F}$53BP1$^{-/-}$ cells expressing MYC-RPA32 treated with zeocin (100 μg/ml, for 1 hour; 2 hours before analysis). (**B**) Percentage of γ-H2AX positive cells in experiments as in (A). (**C**) Percentage of cells [as in (A)] scored positive when containing at least five γ-H2AX foci colocalizing with RPA. (**D**) IF for γH2AX (green) and BARD1 (red) in Rif1$^{F/F}$ and Rif1$^{F/F}$53BP1$^{-/-}$ MEFs. Cells and treatment as in (A). (**E**) Percentage of γ-H2AX-positive cells in experiments in (D). (**F**) Percentage of cells in (D) containing >5 BARD1/γ-H2AX colocalizing foci. (**G**) Examples of misrejoined and radial chromosomes (arrowheads) in BRCA1sh/PARPi-treated Rif1$^{F/F}$ cells with or without Cre. (**H**) Percentages of chromosomes that are misrejoined in the indicated genotypes and treatments. Data in (B), (C), (E), (F), and (H) are means of three to five experiments ±SDs. **, $P < 0.05$ (two-tailed paired Student's *t* test).

Downloaded from www.sciencemag.org on April 12, 2013

end resection. In contrast, Rif1 does not appear to be required for the ability of 53BP1 to promote an increase in the mobility of dysfunctional telomeres. The intermediate effect of Rif1 on the fusion of dysfunctional telomeres can be explained based on these two observations. The increased resection of dysfunctional telomeres in absence of Rif1 is likely to be responsible for the mild inhibition of NHEJ. However, in the absence of 53BP1, the effect of increased resection is combined with a defect in the induction of the mobility of the dysfunctional telomeres, resulting in a more severe blockade to NHEJ. Similarly, we propose that Rif1 deletion leads to partial rescue of chromosome misrejoining in PARPi/BRCA1 shRNA-treated cells because the control of 5′ end resection is only one of multiple mechanisms by which 53BP1 acts. One possibility is that the other mechanism used by 53BP1 in this context, similar to what happens at dysfunctional telomeres, involves the induction of DSB mobility that increases the chance that DSB misrejoining occurs.

References and Notes

1. A. T. Noon, A. A. Goodarzi, *DNA Repair* **10**, 1071 (2011).
2. I. M. Ward, K. Minn, J. van Deursen, J. Chen, *Mol. Cell. Biol.* **23**, 2556 (2003).
3. J. C. Morales *et al.*, *J. Biol. Chem.* **278**, 14971 (2003).
4. S. Difilippantonio *et al.*, *Nature* **456**, 529 (2008).
5. N. Dimitrova, Y. C. Chen, D. L. Spector, T. de Lange, *Nature* **456**, 524 (2008).
6. S. F. Bunting *et al.*, *Cell* **141**, 243 (2010).
7. A. Bothmer *et al.*, *Mol. Cell* **42**, 319 (2011).
8. A. Sfeir, T. de Lange, *Science* **336**, 593 (2012).
9. L. Xu, E. H. Blackburn, *J. Cell Biol.* **167**, 819 (2004).
10. J. Silverman, H. Takai, S. B. Buonomo, F. Eisenhaber, T. de Lange, *Genes Dev.* **18**, 2108 (2004).
11. M. S. Huen *et al.*, *Mol. Cell* **37**, 854 (2010).
12. C. F. Hardy, L. Sussel, D. Shore, *Genes Dev.* **6**, 801 (1992).
13. S. Anbalagan, D. Bonetti, G. Lucchini, M. P. Longhese, *PLoS Genet.* **7**, e1002024 (2011).
14. D. Bonetti *et al.*, *PLoS Genet.* **6**, e1000966 (2010).
15. S. B. Buonomo, Y. Wu, D. Ferguson, T. de Lange, *J. Cell Biol.* **187**, 385 (2009).
16. D. Cornacchia *et al.*, *EMBO J.* **31**, 3678 (2012).
17. S. Yamazaki *et al.*, *EMBO J.* **31**, 3667 (2012).
18. A. A. Sartori *et al.*, *Nature* **450**, 509 (2007).
19. X. Yu, L. C. Wu, A. M. Bowcock, A. Aronheim, R. Baer, *J. Biol. Chem.* **273**, 25388 (1998).
20. A. K. Wong *et al.*, *Oncogene* **17**, 2279 (1998).
21. H. Takai, A. Smogorzewska, T. de Lange, *Curr. Biol.* **13**, 1549 (2003).

Acknowledgments: We thank D. White for expert mouse husbandry and M. Nussenzweig for providing mutant 53BP1 constructs. M.Z. was supported by a Brno Ph.D. talent fellowship and by a grant from the Czech Science Foundation to Ctirad Hofr (P205/12/0550) (see supplementary materials for detailed acknowledgement). This work was supported by a grant from the Breast Cancer Research Foundation to T.d.L. T.d.L. is an American Cancer Society Research Professor.

Supplementary Materials

www.sciencemag.org/cgi/content/full/science.1231573/DC1
Materials and Methods
Figs. S1 to S4
References (*22*–*28*)

16 October 2012; accepted 14 December 2012
Published online 10 January 2013;
10.1126/science.1231573

Regulation of Flowering by Trehalose-6-Phosphate Signaling in *Arabidopsis thaliana*

Vanessa Wahl,[1]* Jathish Ponnu,[2] Armin Schlereth,[1] Stéphanie Arrivault,[1] Tobias Langenecker,[2] Annika Franke,[1] Regina Feil,[1] John E. Lunn,[1] Mark Stitt,[1] Markus Schmid[2]*

The timing of the induction of flowering determines to a large extent the reproductive success of plants. Plants integrate diverse environmental and endogenous signals to ensure the timely transition from vegetative growth to flowering. Carbohydrates are thought to play a crucial role in the regulation of flowering, and trehalose-6-phosphate (T6P) has been suggested to function as a proxy for carbohydrate status in plants. The loss of *TREHALOSE-6-PHOSPHATE SYNTHASE 1* (*TPS1*) causes *Arabidopsis thaliana* to flower extremely late, even under otherwise inductive environmental conditions. This suggests that *TPS1* is required for the timely initiation of flowering. We show that the T6P pathway affects flowering both in the leaves and at the shoot meristem, and integrate *TPS1* into the existing genetic framework of flowering-time control.

The transition from vegetative to reproductive development is an important phase change in a plant's life. When timed correctly, the transition helps to ensure reproductive success and therefore has adaptive value. For this reason, plants have evolved an intricate genetic network that controls the onset of flowering in response to environmental and endogenous signals such as day length, temperature, hormonal status, and carbohydrate availability (*1*). Day length is perceived in the leaves, where a sufficiently long day (i.e., an inductive photoperiod) leads to induction of the *FLOWERING LOCUS T* (*FT*) gene (*2*–*7*). The FT protein functions as a long-distance signal (florigen) that is transported to the shoot meristem, where it interacts with the bZIP transcription factor FD and triggers the formation of flowers (*8*–*11*).

In contrast to the detailed understanding of the photoperiod pathway, relatively little is known about the contribution of carbohydrates to the regulation of flowering (*12*). Mutations in genes of key enzymes in sugar and starch metabolism such as *HEXOKINASE1* (*HXK1*) and *PHOSPHOGLUCOMUTASE1* (*PGM1*) have been shown to affect various aspects of development, including flowering (*13*). A particularly striking example in this respect is TREHALOSE-6-PHOSPHATE SYNTHASE 1 (TPS1), which catalyzes the formation of trehalose-6-phosphate (T6P) from glucose-6-phosphate and uridine diphosphate (UDP)–glucose (*13*, *14*). T6P, which is found only in trace amounts in most plants, has been suggested to function as a signaling molecule that relays information about carbohydrate availability to other signaling pathways (*15*). In agreement with the proposed role of T6P as a central hub in carbon signaling, *TPS1* loss-of-function mutants are embryonic lethal (*16*). Expression of *TPS1* from the seed-specific *ABI3* promoter has been shown to be sufficient to rescue the embryo defect, but the resulting homozygous *tps1 ABI3:TPS1* plants develop slowly and senesce before entering the reproductive phase (*17*). Homozygous *tps1-2* mutants have also been recovered using a chemically inducible rescue construct (*GVG:TPS1*), which enables induction of *TPS1* by dexamethasone application, allowing the *tps1-2 GVG:TPS1* embryos to be rescued to give viable plants that can be stably maintained (*18*). The resulting *tps1-2 GVG:TPS1* plants flower extremely late, producing infertile flowers on shoots that simultaneously arise from the shoot apical meristem (SAM) and axillary meristems, or completely fail to flower, even under inductive photoperiod. These findings indicate that TPS1 plays a critical role in controlling the transition to flowering. However, it is currently unclear where TPS1 is integrated into the canonical flowering-time pathways.

To better understand the molecular function of TPS1, we first confirmed its effect on flowering by knocking down *TPS1* expression with the use of an artificial microRNA (*35S:amiR-TPS1*; figs. S1 and S2) (*19*). This resulted in a significant 25 to 30% reduction in T6P levels (fig. S3) and a delay in flowering by more than 20 leaves (Table 1, experiment 1; fig. S4). In contrast, sucrose levels were significantly higher in *35S:amiR-TPS1* plants (fig. S4), indicating that carbohydrate availability as such was not compromised in those plants. These findings highlight

[1]Department of Metabolic Networks, Max Planck Institute of Molecular Plant Physiology, Am Mühlenberg 1, 14476 Potsdam, Germany. [2]Department of Molecular Biology, Max Planck Institute for Developmental Biology, Spemannstr. 35, 72076 Tübingen, Germany.

*To whom correspondence should be addressed. E-mail: vanessa.wahl@mpimp-golm.mpg.de (V.W.); maschmid@tuebingen.mpg.de (M.S.)

Downloaded from www.sciencemag.org on April 12, 2013